Journal of Biomechanics 82 (2019) 387–391

Contents lists available at ScienceDirect

Journal of Biomechanics

journal homepage: www.elsevier.com/locate/jbiomech
www.JBiomech.com

Short communication

Aerodynamic investigation of the thermo-dependent flow structure in the wake of a cyclist

F. Beaumont [a], P. Lestriez [a], P. Estocq [a], R. Taiar [a,*], F. Grappe [b,c], G. Polidori [a]

[a] GRESPI, Research Group in Engineering Sciences, Université de Reims Champagne-Ardenne, Moulin de la Housse, 51687 Reims cedex 2, France
[b] EA 4660, laboratoire C3S, unité des sports (U-Sports), Université de Franche-Comté, 25000 Besançon, France
[c] Equipe Cycliste Groupama-FDJ, France

ARTICLE INFO

Article history:
Accepted 2 November 2018

Keywords:
Cycling
CFD
Aerodynamic drag
Power output
Temperature

ABSTRACT

The main purpose of this study was to assess the influence of the environmental temperature on both the aerodynamic flow evolving around the bicycle and cycling power output. The CFD method was used to investigate the detailed flow field around the cyclist/bicycle system for a constant speed of 11.1 m/s (40 km/h) without wind. In complement, a mathematical model was used to determine the temperature-dependent power output in the range [−10; 40 °C]. The numerical investigation gives valuable information about the turbulent flow field in the cyclist's wake which evolves accordingly the surrounding temperature. A major result of this study is that the areas of overpressure upstream of the cyclist and of underpressure downstream of him are less extensive for a temperature of 40 °C compared to −10 °C. The results suggest that the aerodynamic braking effect of the bicycle is minimized when the air temperature is high, as a lower air density results in a reduction in drag on the cyclist. This study showed that the power required to maintain a constant speed is reduced when the temperature is high, the reason being a lower aerodynamic resistance.

1. Introduction

International road cycling competitions are organized in many countries around the world (Australia, Belgium, Canada, Emirates, Italy…). Competitors must combine the practice of their sport with the climate of the country in which the competition is held. In some latitudes, races are scheduled during the coldest months of the year and despite this, temperatures sometimes exceed 40 °C. For instance, it was measured 37 °C in the shade at the 2016 World Cycling Championships in Doha and even 46 °C during the Tour of California 2013 (Palm Springs Aerial Tramway stage). Conversely, in the northern hemisphere, temperatures can drop below zero as happened during the Samyn Grand Prix (Quaregnon, Wallonia) where the temperature dropped to −6°C under shelter.

To our knowledge, few studies have focused on the influence of temperature on cycling. Hettinga et al. (2007) found that gross-efficiency was lower in the heat. Others researchers have studied the influence of altitude and varying air density to compare current world cycling records (Bassett et al., 1999; Péronnet et al., 1989). These field measurements have demonstrated a strong link between both air viscosity and density and cycling performance. Such studies are essential but do not allow a thorough analysis of the physics associated with the results of field measurements. In such a case, further analysis are needed to highlight the complex aerodynamic phenomena which are seen to be temperature dependent.

On the other hand, studying the flow structure around a bicycle may be a real technological challenge. Computational Fluid Dynamics (CFD) can be a valuable alternative to the use of expensive experimental techniques. The CFD has grown rapidly in recent years; its use in sports (bobsleigh, cycling, swimming, skating, ski jumping, wheelchair sprinting…) has become widespread and numerous studies have shown its potential (Forte et al., 2018; Sciacchitano & Pattnaik, 2018; Beaumont et al., 2017; Bixler et al., 2007; Gardan et al., 2017; Hart et al., 2010; Loebbecke et al., 2009; Popa, et al., 2011; Zaïdi et al., 2010).

To the best of our knowledge, the CFD approach is used for the first time to investigate the influence of surrounding temperature on the aerodynamic flow evolving around the bicycle. The main aim of this paper is to numerically investigate the aerodynamic phenomena that are intrinsically linked to thermo-dependent parameters such as physico-chemical air properties (density, viscosity). In complement, a mathematical model was used to

* Corresponding author.
E-mail address: redha.taiar@univ-reims.fr (R. Taiar).

https://doi.org/10.1016/j.jbiomech.2018.11.006
0021-9290/

determine the temperature-dependent power output in the range [−10; 40 °C]. The numerical investigation was carried-out using a commercial CFD code based on the finite volume method. The temperature range investigated (−10 °C to 40 °C) is consistent with the temperatures recorded during international level cycling competitions. A speed of 11.1 m/s (40 km/h) has been used, corresponding to an average speed in road cycling competition.

2. CFD methods

A top-10 Grand Tour cycling finisher (1.8 m, 63 kg) volunteered to take part of the study. The CAD model of the cyclist used in our study was achieved using a laser scanner (high resolution laser scanner, ROMER®) which provided all the dimensional characteristics of the cyclist in a time trial position. More details on the cyclist's scanning are available in a previous article (Beaumont et al., 2018).

The size of the computational domain as well as the meshing method are carefully described in a previous study as well as a grid dependency test which was performed to ascertain the independence of the mesh size with respect to the results (Beaumont et al., 2018).

The ANSYS Fluent 18.2® commercial CFD code was used to solve the three-dimensional flow around the cyclist and bicycle setup. The Reynolds averaged Navier-Stokes (RANS) equations were solved with the standard turbulence model k-ω. The k-ω model has been used on many sports-related studies such as swimming (Beaumont et al., 2017, Mantha et al., 2014; Zaïdi et al., 2010), cycling (Defraeye et al., 2010; Mannion et al., 2017) or skateboarding (Hart et al., 2010). Convergence of the results was verified by monitoring the drag coefficients at each time step and was obtained when their value no longer changed over time.

Mathematical formulation of the CFD model is outlined in Appendix A

2.1. Boundary conditions

We applied a constant speed of 11.1 m/s (40 km/h) at the entrance to the calculation area, which corresponds to an average speed of a cycling race. Others boundary conditions are discussed in a previous article (Beaumont et al., 2018). In order to assess the influence of air temperature on the aerodynamic drag of the cyclist and bicycle system, calculations were performed in the temperature range [−10 °C; 40 °C].

2.2. Predicting power output versus temperature

From the aerodynamic (CFD) drag values and mechanical variables, we can estimate the cycling power output using a mathematical model. On a flat terrain, power output is the sum of aerodynamic resistance, rolling resistance and resistance due to mechanical friction. Millet et al (2014) used a well-known biomechanical model that combines the powers needed to overcome aerodynamic drag, rolling resistance or friction of the bicycle's mechanical components.

For a flat terrain, the power output $\bar{P}_{ext}$ can be described by the following equation:

$$\bar{P}_{ext} = P_{aero} + P_{roll} + P_{fri} \quad (1)$$

The first term corresponds to the power used to overcome air resistance, the second term is related to mechanical friction generated to a large extent by tyre friction on the road and the last term corresponds to the friction of the mechanical elements of the bicycle (www.friction-facts.com).

The Eq. (1) can be written as follows:

$$\bar{P}_{ext} = 0.5\rho A C_D \bar{V}_C^{\,3} + C_r M g \bar{V}_C + F_b \quad (2)$$

$\bar{V}_C$ is the velocity of the bicycle (m/s). R_r is defined as the rolling resistance and$R_r = C_r Mg$; C_r being the rolling coefficient depending on the tyre deformation magnitude.M is the mass of the cyclist/bicycle system (kg), the acceleration of gravity g is equal to 9.81 m·s^{-2}. F_b is the friction associated with drive-train transmission.

The mass of the cyclist/bicycle system was estimated at 71 Kgs. We used a frontal area of 0.39 m^2 corresponding to the cyclist and his bicycle in aero position. Moreover, we estimated the power relative to friction losses at about 7 W (www.friction-facts.com). We used a rolling coefficient$C_r = 0.0025$, this value being estimated according to the works of Grappe et al. (1999).

3. Results and discussion

In practice, it is possible for coaches and cyclists to specify training objectives based on the estimated total power. Road cycling power can be assessed using aerodynamic resistance, rolling resistance and resistance due to mechanical friction. Aerodynamic drag which was deduced from numerical results, has been identified as a prevailing term, requiring up to 96% of the cyclist's power (Martin et al., 1998). In this study, we found that aerodynamic drag decrease as ambient temperature increase. Afterwards, we implemented the drag values in a mathematical model in order to estimate the evolution of the cyclist's power as a function of the environmental temperature. Results have shown that at a constant speed (40 km/h), power output declined in a linear fashion (r = 0.53) as environmental temperature rise.

$$\left|\frac{dP}{dt}\right| = -0.53\,\mathrm{W/^{\circ}C} \quad (3)$$

For instance, mathematical model predicts a 13% decrease in power when the temperature increases from −10 °C to 40 °C.

Based on the statement that aerodynamic drag is a predominant parameter, a more detailed analysis seemed necessary to improve our knowledge on the aerodynamic flow structure evolving around the bicycle. It has been found that a shift in the thermophysical properties of the ambient air consequently alters the distribution of pressure and velocity in the cyclist's wake. Fig. 1 shows the pressure distribution on the cyclist's body and in the surrounding air for a temperature Tair = −10 °C and Tair = 40 °C. In order to highlight the areas of overpressure and underpressure, we have deliberately restricted the values to the range [−100; 100 Pa] and [−20; 40 Pa] even if the min and max values are higher.

The pressure maps presented for the two temperatures allow us to highlight strong differences in the pressure distribution as well as in the pressure values indicated by arrows on the figure. If we compare the pressures in a selected area of the cyclist's body, we can see that the overpressure or underpressure values decrease as the air temperature increases (a, b).

The pressure distribution in the surrounding air (c, d) evidences that the zones of overpressure upstream of the cyclist (colored in red) and of underpressure downstream of him (colored in dark blue) are less extensive at T_{air} = 40 °C in comparison with T_{air} = −10 °C. A modification of the pressure field around the cyclist implies changes in the flow velocity field located in the wake of the cyclist. It can be stated that most of the shear stresses of a gas are due to molecular transfer. As a result, the higher the temperature, the greater the transfer, as molecules move faster. Thus, the braking effect of the bicycle due to the aerodynamic drag will be less when the air temperature is high. Finally, a lower air density results in a reduction in aerodynamic drag on the cyclist.

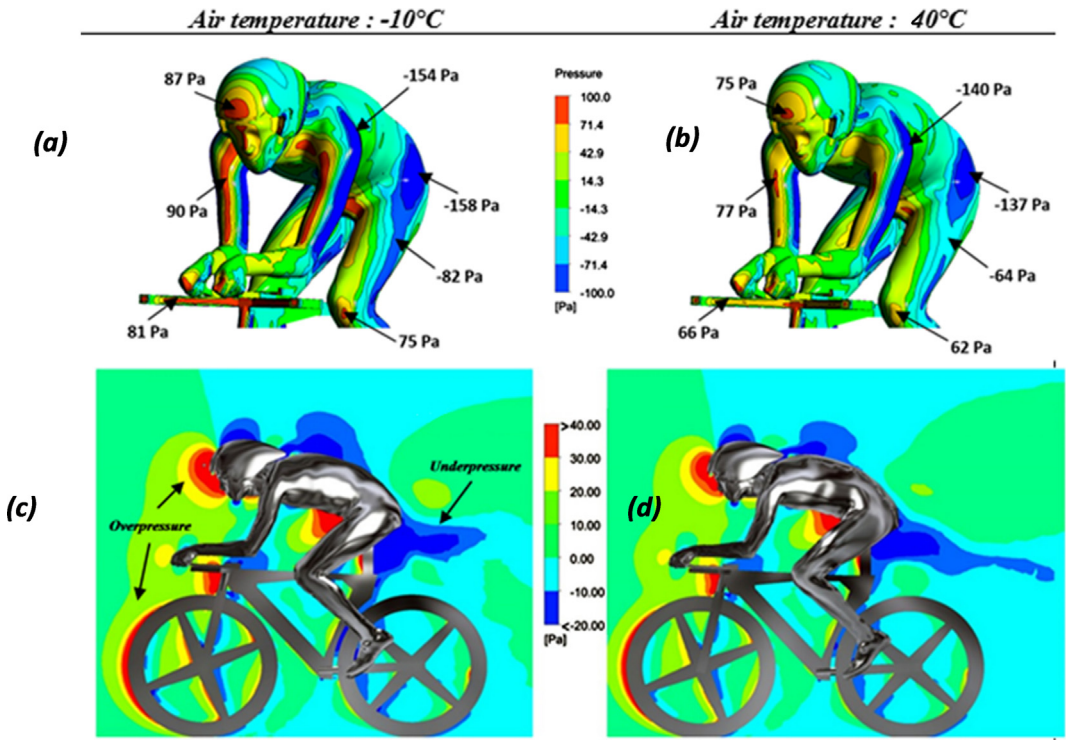

Fig. 1. (a and b) Maps of the pressure applied on the cyclist's body for T = −10 °C (a) and T = 40 °C (b) and a speed U = 11.1 m·s^{-1}; (c and d) Pressure distribution in the surrounding air around the bicycle/cyclist system and displayed in a vertical centerplane for a temperature Tair = −10 °C (a) and Tair = 40 °C (b) and a speed U = 11.1 m·s^{-1}.

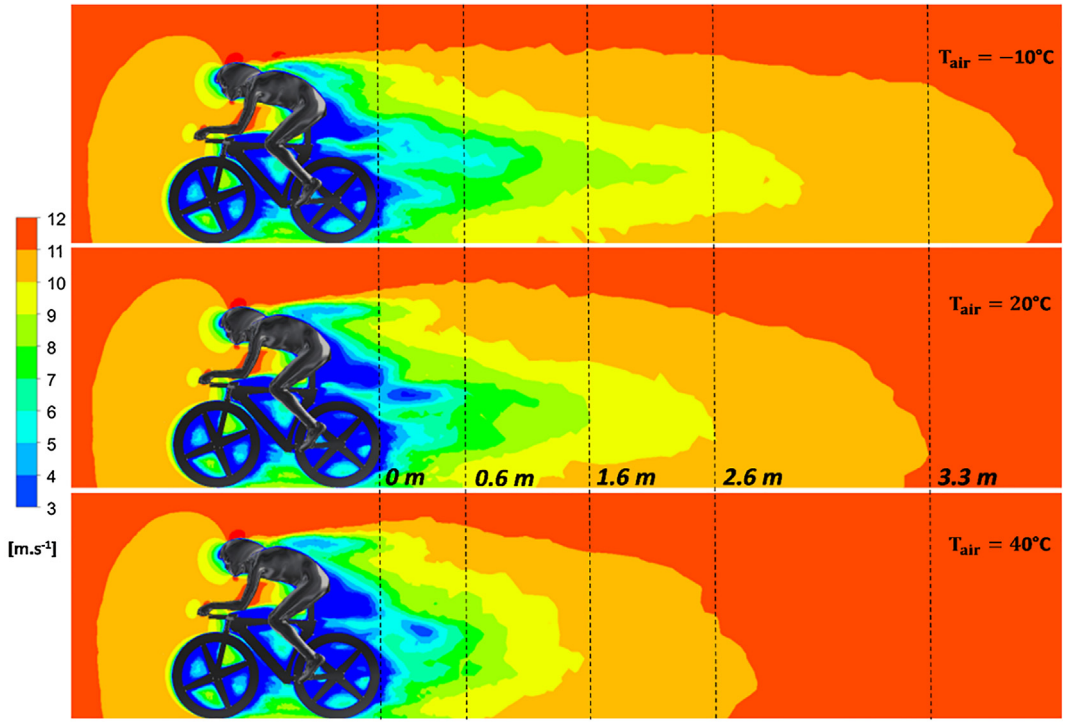

Fig. 2. Axial velocity contours in the surrounding air around the bicycle/cyclist system displayed in a vertical centerplane for T = −10, 20 and 40 °C and for a speed U = 11.1 m·s^{-1}. The broken lines are used to determine the wake length.

Fig. 2 shows the axial velocity contours of the flow around the bicycle/cyclist system displayed in a vertical centerplane for T = −10, 20 and 40 °C. Fig. 2 indicates that the length of the wake behind the cyclist decreases as the air temperature increases. The wake length is greater than 3.3 m at a temperature of −10 °C compared to approximately 2.7 m at a temperature of 40 °C. It is worth noting that the larger the wake, the greater the area over which the pressure difference between the front and back of the body acts,

resulting in a greater drag (Douglas et al., 2005). Our results demonstrates that in order to minimize pressure drag, it is important to reduce the size of the wake. Fig. 2 indicates that the velocity of the fluid in the wake is greatly reduced with respect to that upstream of the bicycle/cyclist system. According to the so-called Bernoulli's equation, there is an inverse relationship between pressure and velocity. As seen on Figs. 1 and 2, the lower the velocity, the higher the pressure.

4. Conclusion

The main aim of this paper was to numerically investigate the turbulent flow field in the wake of the cyclist whose behavior is intrinsically linked to the physico-chemical air parameters which are highly temperature-dependent. The CFD method was used to model the aerodynamic behavior of the cyclist and bicycle system for a speed of 40 km/h without wind and for environmental temperatures between −10 °C and 40 °C. Numerical results showed for example that an increase in air temperature not only affects the pressure values on the cyclist's body, but also the velocity field of the flow in the cyclist's wake. In complement of this aerodynamic investigation, we used a mathematical model to predict the temperature-dependent power output. This can be useful in practice as coaches and cyclists can specify training objectives based on the total power estimate. Finally, results from this study suggested that riding in a warmer environment increase the cyclist's travel speed by reducing both aerodynamic braking effect and drag forces. However, this result must be qualified because the cyclist's ability to maintain his power output may be impaired in case of severe heat. Future studies are expected to investigate the influence of various environmental conditions (humidity, wind, altitude, etc.) on the aerodynamic drag of the cyclist and bicycle system.

Conflict of interest statement

The authors declare that they don't have any financial and personal relationships with other people or organizations that could inappropriately influence (bias) their work.

Appendix A

Mean-Flow equations

Conservation of mass, momentum, and energy are expressed by the Favre-averaged equations (Wilcox, 2008):

$$\frac{\partial \rho}{\partial t}+\frac{\partial}{\partial x_i}(\rho.u_i)=0 \tag{1}$$

$$\frac{\partial}{\partial t}(\rho.u_i)+\frac{\partial}{\partial x_j}(\rho.u_j.u_i)=-\frac{\partial p}{\partial x_i}+\frac{\partial}{\partial x_j}(t_{ji}+\rho.\tau_{ji}) \tag{2}$$

$$\frac{\partial}{\partial t}\left[\rho\left(e+\frac{1}{2}u_i.u_i+k\right)\right]+\frac{\partial}{\partial x_j}\left[\rho.u_j\left(h+\frac{1}{2}u_i.u_i+k\right)\right] = \frac{\partial}{\partial x_j}\left[u_i(t_{ij}+\rho.\tau_{ij})+\left(\frac{\mu}{Pr_L}+\frac{\mu_T}{Pr_T}\right)\frac{\partial h}{\partial x_j}+\left(\mu+\sigma^*\frac{\rho.k}{\omega}\right)\frac{\partial k}{\partial x_j}\right] \tag{3}$$

Constitutive equations

The following equations are used by the model to compute the molecular and specific Reynolds-stress tensors (Wilcox, 2008):

$$t_{ij}=2\mu.\bar{S}_{ij},\ \rho.\tau_{ij}=2\mu_T.\bar{S}_{ij}-\frac{2}{3}\rho.k.\delta_{ij} \tag{4}$$

$$\bar{S}_{ij}=S_{ij}-\frac{1}{3}\frac{\partial u_k}{\partial x_k}\delta_{ij} \tag{5}$$

$$\mu_T=\frac{\rho.k}{\omega},\quad \omega=max\left\{\omega, C_{lim}\sqrt{\frac{2\bar{S}_{ij}.\bar{S}_{ij}}{\beta^*}}\right\} \tag{6}$$

$$C_{lim}=\frac{7}{8} \tag{7}$$

Turbulence

The turbulence kinetic energy and specific dissipation rate can be described by the following equations:

$$\frac{\partial}{\partial t}(\rho.k)+\frac{\partial}{\partial x_j}(\rho.u_j.k)=\rho.\tau_{ij}\frac{\partial u_i}{\partial x_j}-\beta^*.\rho.k.\omega + \frac{\partial}{\partial x_j}\left[\left(\mu+\sigma^*\frac{\rho.k}{\omega}\right)\frac{\partial k}{\partial x_j}\right] \tag{8}$$

$$\frac{\partial}{\partial t}(\rho.\omega)+\frac{\partial}{\partial x_j}(\rho.u_j.\omega)=\alpha\frac{\omega}{k}\rho.\tau_{ij}\frac{\partial u_i}{\partial x_j}-\beta.\rho.\omega^2+\sigma_d\frac{\rho}{\omega}\frac{\partial k}{\partial x_j} \times\frac{\partial \omega}{\partial x_j}+\frac{\partial}{\partial x_j}\left[\left(\mu+\sigma\frac{\rho.k}{\omega}\right)\frac{\partial \omega}{\partial x_j}\right] \tag{9}$$

Closure coefficients

The various closure coefficients are:

$$\alpha=\frac{13}{25},\ \beta^*=\frac{9}{100},\ \sigma=\frac{1}{2},\ \sigma^*=\frac{3}{5},\ Pr_T=\frac{8}{9} \tag{10}$$

$$\sigma_d=\begin{cases}0, & \frac{\partial k}{\partial x_j}\frac{\partial \omega}{\partial x_j}\le 0\\ \sigma_{d0}, & \frac{\partial k}{\partial x_j}\frac{\partial \omega}{\partial x_j}>0\end{cases},\quad \sigma_{d0}=\frac{1}{8} \tag{11}$$

$$\beta=\beta_0.f_\beta,\quad \beta_0=0.0708,\quad f_\beta=\frac{1+85\chi_\omega}{1+100\chi_\omega} \tag{12}$$

$$\chi_\omega\equiv\left|\frac{\Omega_{ij}.\Omega_{jk}.\widehat{S}_{ki}}{(\beta^*.\omega)^3}\right|,\quad \widehat{S}_{ki}=S_{ki}-\frac{1}{2}\frac{\partial u_m}{\partial x_m}\delta k_i \tag{13}$$

The round-jet parameter χ_ω is calculated with$\widehat{S}_{ki}$, which, contrary to the compressible deformation rate recommended by Papp & Dash (2001), is Galilean invariant.

Appendix B. Supplementary material

Supplementary data to this article can be found online at https://doi.org/10.1016/j.jbiomech.2018.11.006.

References

Bassett, D.R., Kyle, C.R., Passfield, L., Broker, J.P., Burke, E.R., 1999. Comparing cycling world hour records, 1967–1996: modeling with empirical data. Med. Sci. Sports Exe. 31, 1665–1676.

Beaumont, F., Taiar, R., Polidori, G., Trenchard, H., Grappe, F., 2018. Aerodynamic study of time-trial helmets in cycling racing using CFD analysis. J. Biomech. 67, 1–8.

Beaumont, F., Taïar, R., Polidori, G., 2017. Preliminary numerical investigation in open currents-water swimming: pressure field in the swimmer wake. Appl. Math. Comput. 302, 48–57.

Bixler, B., Pease, D., Fairhurst, F., 2007. The accuracy of computational fluid dynamics analysis of the passive drag of a male swimmer. Sports Biomech. 6, 81–98.

Defraeye, T., Blocken, B., Koninckx, E., Hespel, P., Carmeliet, J., 2010. Computational fluid dynamics analysis of cyclist aerodynamics: performance of different turbulence-modelling and boundary-layer modelling approaches. J. Biomech. 43, 2281–2287.

Douglas, J.F., Gasiorek, J.M., Swaffield, J.A., Jack, L.B., 2005. Fluid Mechanics. Pearson Education.

Forte, P., Marinho, D.A., Morais, J.E., Morouço, P.G., Barbosa, T.M., 2018. The variations on the aerodynamics of a world-ranked wheelchair sprinter in the key-moments of the stroke cycle: a numerical simulation analysis. PLOS ONE 13 (2), e0193658.
Gardan, N., Schneider, A., Polidori, G., Trenchard, H., Seigneur, J.M., Beaumont, F., Fourchet, F., Taiar, R., 2017. Numerical investigation of the early flight phase in ski-jumping. J. Biomech. 59, 29–34.
Grappe, F., Candau, R., Barbier, B., Hoffman, M.D., Belli, A., Rouillon, J.-D., 1999. Influence of tyre pressure and vertical load on coefficient of rolling resistance and simulated cycling performance. Ergonomics 42, 1361–1371.
Hart, J.H., Allen, T., Holroyd, M., 2010. Downhill skateboard aerodynamics. Proc. Eng. 2, 2523–2528.
Hettinga, F.J., De Koning, J.J., de Vrijer, A., Wüst, R.C.I., Daanen, H.A.M., Foster, C., 2007. The effect of ambient temperature on gross-efficiency in cycling. Euro. J. Appl. Physiol. 101, 465–471.
Loebbecke, A.V., Mittal, R., Mark, R., Hahn, J., 2009. A computational method for analysis of underwater dolphin kick hydrodynamics in human swimming. Sports Biomech. 8, 60–77.
Mannion, P., Toparlar, Y., Blocken, B., Hajdukiewicz, M., Andrianne, T., Clifford, E., 2017. Improving CFD prediction of drag on Paralympic tandem athletes: influence of grid resolution and turbulence model. Sports Eng. 21, 1–13.
Mantha, V.R., Marinho, D.A., Silva, A.J., Rouboa, A.I., 2014. The 3D CFD study of gliding swimmer on passive hydrodynamics drag. Braz. Arch. Biol. Technol. 57, 302–308.
Martin, J.C., Milliken, D.L., Cobb, J.E., McFadden, K.L., Coggan, A.R., 1998. Validation of a mathematical model for road cycling power. J. Appl. Biomech. 14, 276–291.
Millet, G.P., Tronche, C., Grappe, F., 2014. Accuracy of indirect estimation of power output from uphill performance in cycling. Int. J. Sports Physiol. Perform. 9, 777–782.
Papp, J.L., Dash, S.M., 2001. Turbulence Model Unification and Assessment for High-Speed Aeropropulsive Flows. AIAA Paper 2001-10880.
Péronnet, F., Bouissou, P., Perrault, H., Ricci, J., 1989. A comparison of cyclists' time records according to altitude and materials used. Can. J. Sport Sci. 14, 93–98.
Popa, C.V., Zaidi, H., Arfaoui, A., Polidori, G., Taiar, R., Fohanno, S., 2011. Analysis of wall shear stress around a competitive swimmer using 3D Navier-Stokes equations in CFD. Acta Bioeng. Biomech. 13, 3–11.
Sciacchitano, A., Pattnaik, P., 2018. Near wake analysis of a two-man bobsleigh. Scaled Model. Proc. 2, 319.
Wilcox, D.C., 2008. Formulation of the k-w turbulence model revisited. AIAA J. 46, 2823–2838.
Zaïdi, H., Fohanno, S., Taïar, R., Polidori, G., 2010. Turbulence model choice for the calculation of drag forces when using the CFD method. J. Biomech. 43, 405–411.